doi:10.3969/j.issn.1001-893x.2013.01.019

Hybrid FEM-FIPWA for Scattering from Complex Bodies of Revolution*

RUI Xi[1,**], HU Jun[2], LIU Qing-huo[3]

(1. Southwest China Institute of Electronic Technology, Chengdu 610036, China;
2. School of Electronic Engineering, University of Electronic Science and Technology of China, Chengdu 610054, China; 3. Department of Electrical and Computer Engineering, Duke University, Durham, NC 27708, USA)

Abstract: A method based on hybrid finite element method (FEM) and fast inhomogeneous plane wave algorithm (FIPWA) is proposed to solve the electromagnetic scattering problem for bodies of revolution (BOR) with inhomogeneous, composite materials. The FEM with mixed edge-based and node-based elements is used for representing the interior electric field, while the FIPWA is used as the exact boundary condition, hybrid triangular and pulse basis functions are used for representing the electric field and magnetic field on the boundary. Both the memory and CPU time requirements are reduced for large scale BOR problems. Numerical results are given to demonstrate the validity and the efficiency of the proposed method.

Key words: composite material; body of revolution; electromagnetic scattering; fast inhomogeneous plane wave algorithm; finite element method

中图分类号:TN　　**文献标志码**:A　　**文章编号**:1001-893X(2013)01-0093-06

混合FEM-FIPWA求解复杂旋转体散射

芮　锡[1],胡　俊[2],柳清伙[3]

(1.中国西南电子技术研究所,成都 610036;2.电子科技大学 电子工程学院,成都 610054;
3.杜克大学 电气和计算机工程学院,达勒姆 27708,美国)

摘　要:提出了一种基于混合有限元与快速非均匀平面波算法求解复杂旋转体的散射问题。内部电场采用基于点元和边元基函数的有限元方法计算,同时在旋转体的外表面的场采用基于三角基函数及脉冲基函数的快速非均匀平面波算法计算。采用这种方法处理复杂大尺度的旋转体问题能节省计算的内存和计算时间,算例验证了算法的准确性和有效性。

关键词:复合材料;旋转体;电磁散射;快速非均匀平面波算法;有限元法

1 Introduction

The electromagnetic problem for bodies of revolution (BOR) of arbitrary shape with different kinds of materials has been widely discussed for several decades[1-6]. In this work, FEM-BI is presented to analyze the scattering of BOR with inhomogeneous materials, and extend the fast inhomogeneous plane wave algorithm to accelerate the computation of the method of moment (MoM). Finite Element Method (FEM) is used to analyze the interior electric field. Edge-based and node-based elements are used to represent the interior electric field. While for the exterior region, Boundary Integration (BI) is used as a exact boundary condition. Triangular and pulse basis functions are used to represent the electric and magnetic fields on the boundary. The aggregation and disaggregation factors in Fast Inhomogeneous Plane Wave Algorithm (FIPWA) can be derived analytically. Both the memory requirement and the CPU time are saved for large scale BOR prob-

* Received date: 2012-11-28; Revised date: 2012-12-13　收稿日期:2012-11-28;修回日期:2012-12-13
** **Corresponding author**: uestcruixi@gmail.com　**通讯作者**:uestcruixi@gmail.com

lems. Numerical results are given to demonstrate the validity and the efficiency of the presented method.

2 FEM-FIPWA for Axisymmetric Resonators

2.1 Body of revolution

Because of the symmetry of the geometry, the volume of the BOR is generated by revolving a plane curve about the z-axis as shown in Figure 1. Here (ρ, ϕ, z) are the variables in cylindrical coordinate system, θ^{inc} is the angle of incident wave, $\hat{t}$ and $\hat{\phi}$ are the unit vectors, S is the surface of the BOR.

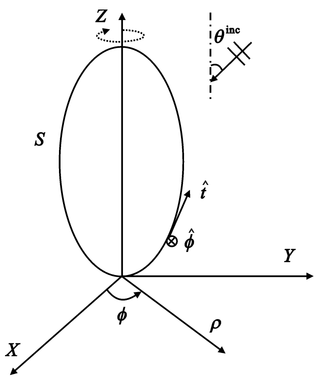

Fig. 1 Body of revolution and coordinate system
图 1 旋转体结构坐标系统

The electric and magnetic fields can be expressed in a Fourier series:

$$\boldsymbol{E}(\rho,\phi,z) = \sum_{m=-\infty}^{\infty}[\boldsymbol{E}_{t,m}(\rho,z) + \hat{\phi}\boldsymbol{E}_{\phi,m}(\rho,z)]\mathrm{e}^{\mathrm{j}m\phi} \tag{1}$$

$$\boldsymbol{H}(\rho,\phi,z) = \sum_{m=-\infty}^{\infty}[\boldsymbol{H}_{t,m}(\rho,z) + \hat{\phi}\boldsymbol{H}_{\phi,m}(\rho,z)]\mathrm{e}^{\mathrm{j}m\phi} \tag{2}$$

where $\boldsymbol{E}_{t,m}$, $\boldsymbol{E}_{\phi,m}$, $\boldsymbol{H}_{t,m}$ and $\boldsymbol{H}_{\phi,m}$ are the electric and magnetic fields in the meridian plane and the azimuthal component of the m-th Fourier mode, respectively. As the fields are decomposed into two parts as shown in Equation (1–2), only a 2–D mesh (meridian cross section) is needed for analyzing the 3–D axisymmetric problem. These different modes can be treated separately because of the orthogonality. In the cylindrical coordinate system, the unit vectors $\hat{t}$ and $\hat{\phi}$ are defined as

$$\hat{t} = \sin\theta\cos\phi\hat{\boldsymbol{x}} + \sin\theta\sin\phi\hat{\boldsymbol{y}} + \cos\theta\hat{\boldsymbol{z}} \tag{3}$$

$$\hat{\phi} = -\sin\phi\hat{\boldsymbol{x}} + \cos\phi\hat{\boldsymbol{y}} \tag{4}$$

where θ is the angle between the z-axis and the unit vector $\hat{t}$. ϕ is the azimuthal angle as shown in Figure 1.

2.2 FEM for the interior region

As shown in Figure 2, the interior region of the BOR is filled with inhomogeneous material with the relative permittivity ε_r and the relative permeability μ_r. Both ε_r and μ_r are the function of z and ρ, but independent of ϕ.

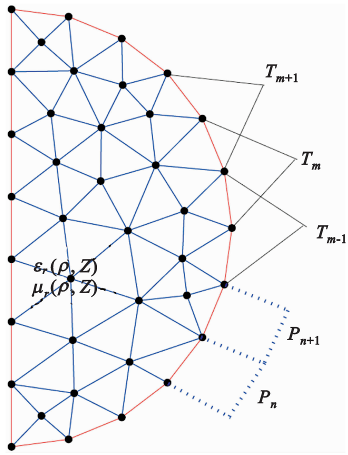

Fig. 2 The mesh for the interior and exterior regions
图 2 内部区域与外部区域的网格划分

The vector Helmholtz equation for the electric field can be written as

$$-\nabla\times(\mu_r^{-1}\nabla\times\boldsymbol{E}) + k_0^2\varepsilon_r\boldsymbol{E} = \mathrm{j}\omega\mu_0\boldsymbol{J} + \nabla\times\mu_r^{-1}\boldsymbol{M} \equiv \boldsymbol{S}_e \tag{5}$$

where $\boldsymbol{S}_e$ is the source term, and k_0 is the wave number in free space. If it is source free ($\boldsymbol{S}_e = 0$) in the interior region the weak form of the vector wave equation can be expressed as[7–8]

$$\int_{\Omega}(\nabla\times\boldsymbol{W}_l)\cdot(\mu_r^{-1}\nabla\times\boldsymbol{E})\mathrm{d}\Omega - \int_{\Omega}k_0^2\boldsymbol{W}_l\cdot\varepsilon_r\boldsymbol{E}\mathrm{d}\Omega = \mathrm{j}\omega\mu_0\int\boldsymbol{W}_l\cdot(\hat{n}\times\boldsymbol{H})\mathrm{d}S \tag{6}$$

where $\boldsymbol{W}_l$ is the testing function, and μ_0 is the permeability of the free space.

The fields must retain the continuity for any values of ϕ on the z-axis ($\rho = 0$). Thus, there are three kinds of conditions for different cylindrical modes:

$$\begin{cases} E_{\phi,0} = E_{\rho,0} = 0, & E_{z,0} \neq 0, \quad m = 0 \\ E_{\rho,\pm 1} = \mp\mathrm{j}E_{\phi,\pm 1}, & E_{z,0} = 0, \quad |m| = 1 \\ E_{\phi,0} = E_{\rho,0} = E_{z,0} = 0, & \quad |m| > 1 \end{cases} \tag{7}$$

The basis functions for the electric field are chosen as

$$E_{\phi,m} = \sum_{i=1}^{N_n} e_{\phi,i} \frac{N_i}{\rho} \quad (8)$$

$$\boldsymbol{E}_{t,m} = \sum_{i=1}^{N_s} e_{t,i} \boldsymbol{N}_i \quad (9)$$

where N_n is the number of nodes, N_s is the number of segments (or edges), $e_{t,i}$ and $e_{\phi,i}$ are the unknown coefficients, and N_i and $\boldsymbol{N}_i$ represent the standard node-based and edge-based element basis functions, respectively. The magnetic field on the boundary S is expanded as the same as the electric field.

$$H_{\phi,m} = \sum_{i=1}^{N_n} h_{\phi,i} \frac{N_i}{\rho} \quad (10)$$

$$\boldsymbol{H}_{t,m} = \sum_{i=1}^{N_s} h_{t,i} \boldsymbol{N}_i \quad (11)$$

The testing function is chosen as

$$\boldsymbol{W}_l = \left(\sum_{i=1}^{N_n} N_i \hat{\phi} + \sum_{i=1}^{N_s} \boldsymbol{N}_i\right) \mathrm{e}^{\mathrm{j}l\phi} = W_{\phi,k} \hat{\phi} + \boldsymbol{W}_{t,l} \quad (12)$$

After substituting the basis and testing functions into Equation (6) and making use of the orthogonality of cylindrical modes, the wave equation can be rewritten as

$$\begin{aligned} &2\pi \int_S \frac{\rho}{\mu_r} (\nabla_t \times \boldsymbol{W}_{t,-m}) \cdot (\nabla_t \times \boldsymbol{E}_{t,-m}) \mathrm{d}S + \\ &2\pi \int_S \frac{\rho}{\mu_r} \left(\nabla_t \times W_{\phi,-m} + \frac{\mathrm{j}m}{\rho} \boldsymbol{W}_{t,-m} + \frac{\hat{\rho}}{\rho} W_{\phi,-m}\right) \cdot \\ &\left(\nabla_t E_{\phi,m} + \frac{-\mathrm{j}m}{\rho} \boldsymbol{E}_{t,m} + \frac{\hat{\rho}}{\rho} E_{\phi,m}\right) \mathrm{d}S - \\ &2\pi \int_S k_0^2 \varepsilon_r (\boldsymbol{W}_{t,-m} \cdot \boldsymbol{E}_{t,m} + W_{\phi,-m} \cdot E_{\phi,m}) \mathrm{d}S - \\ &2\pi \int_S \mathrm{j}\omega\mu_0 \rho (\boldsymbol{W}_{t,-m} + \hat{\phi} W_{\phi,-m}) \cdot \\ &[\hat{n} \times (\hat{\phi} H_{t,m} + \boldsymbol{H}_{t,m})] \mathrm{d}S = 0 \end{aligned} \quad (13)$$

A system of equations

$$\begin{bmatrix} A_m^{tt} & A_m^{t\phi} \\ A_m^{\phi t} & A_m^{\phi\phi} \end{bmatrix} \cdot \begin{bmatrix} e^t \\ e^\phi \end{bmatrix} + \begin{bmatrix} G_m^{tt} & G_m^{t\phi} \\ G_m^{\phi t} & G_m^{\phi\phi} \end{bmatrix} \cdot \begin{bmatrix} h_b^t \\ h_b^\phi \end{bmatrix} = 0 \quad (14)$$

can be formed, where m is the index of the mode and b is the index of boundary. And the matrix element can be expressed as

$$\begin{aligned} A_{mij}^{\alpha\beta} = &\sum_{e=1}^{K} \int_{S_e} (\nabla \times \boldsymbol{W}_{-m}^{\alpha}) \cdot (\mu_r^{-1} \nabla \times \boldsymbol{E}_m^{\beta}) - \\ &k_0^2 \varepsilon_r \boldsymbol{W}_{-m}^{\alpha} \boldsymbol{E}_m^{\beta} \mathrm{d}S \end{aligned} \quad (15)$$

$$G_{mij}^{\alpha\beta} = -\mathrm{j}\omega\mu_0 \sum_{e=1}^{K_b} \boldsymbol{W}_{-m}^{\alpha} \cdot (\hat{n} \times \boldsymbol{E}_m^{\beta}) \mathrm{d}S \quad (16)$$

where α and β are the choices for the testing function and the basis function. $\boldsymbol{e}^t = (e_{t,1}, e_{t,2}, \cdots, e_{t,N_s})^{\mathrm{T}}$, $\boldsymbol{e}^\phi = (e_{\phi,1}, e_{\phi,2}, \cdots, e_{\phi,N_n})^{\mathrm{T}}$, $\boldsymbol{h}_b^t = (h_{t,1}, h_{t,2}, \cdots, h_{t,N_s^b})^{\mathrm{T}}$, and $\boldsymbol{h}_b^\phi = (h_{\phi,1}, h_{\phi,2}, \cdots, h_{\phi,N_n^b})^{\mathrm{T}}$. K is the total number of the elements, K_b is the number of the boundary elements.

A seven-point numerical integration is used for the impedance matrix assembling. The unknowns contain six parts, the interior electric field e_t^i and e_ϕ^i, the boundary electric field e_t^b and e_ϕ^b, the boundary magnetic field h_t^b and h_ϕ^b. The matrix equation for FEM part can be rewritten as

$$\begin{bmatrix} A_{tt}^{ii} & A_{t\phi}^{ii} & A_{tt}^{ib} & A_{t\phi}^{ib} & 0 & 0 \\ A_{\phi t}^{ii} & A_{\phi\phi}^{ii} & A_{\phi t}^{ib} & A_{\phi\phi}^{ib} & 0 & 0 \\ A_{tt}^{bi} & A_{t\phi}^{bi} & A_{tt}^{bb} & A_{t\phi}^{bb} & G_{tt}^{bb} & G_{t\phi}^{bb} \\ A_{\phi t}^{bi} & A_{\phi\phi}^{bi} & A_{\phi t}^{bb} & A_{\phi\phi}^{bb} & G_{\phi t}^{bb} & G_{\phi\phi}^{bb} \end{bmatrix} \cdot \begin{bmatrix} e_t^i \\ e_\phi^i \\ e_t^b \\ e_\phi^b \\ h_t^b \\ h_\phi^b \end{bmatrix} = 0 \quad (17)$$

2.3 FIPWA for the exterior region

For the exterior region, boundary integration is applied to govern the boundary electricfield $\boldsymbol{E}$ and magnetic fields $\boldsymbol{M}$. The fields on the boundary S can be written as

$$\boldsymbol{J} = \hat{n} \times \boldsymbol{H} \quad (18)$$

$$\boldsymbol{M} = -\hat{n} \times \boldsymbol{E} \quad (19)$$

where $\boldsymbol{J}$ and $\boldsymbol{M}$ are the equivalent electric and magnetic currents, which will satisfy the electric field integral equation (EFIE) and the magnetic field integral equation (MFIE)

$$\hat{n} \times \boldsymbol{E}^i = \hat{n} \times L(\bar{\boldsymbol{J}}) - \hat{n} \times \tilde{K}(\boldsymbol{M}) - \frac{1}{2} \boldsymbol{M} \quad (20)$$

$$\hat{n} \times \bar{\boldsymbol{H}}^i = \hat{n} \times \tilde{K}(\bar{\boldsymbol{J}}) + \frac{1}{2} \bar{\boldsymbol{J}} + \hat{n} \times L(\boldsymbol{M}) \quad (21)$$

where $\boldsymbol{E}^i$ and $\boldsymbol{H}^i$ are the incident electric and magnetic fields, $\bar{\boldsymbol{H}}^i = \eta_0 \boldsymbol{H}^i$, $\bar{\boldsymbol{J}} = \eta_0 \boldsymbol{J}$, η_0 is the wave impedance in the free space, L and $\tilde{K}$ are the operators which can be expressed as

$$L(\boldsymbol{x}) = \mathrm{j}k_0 \int_s \left[\boldsymbol{x} + \frac{1}{k_0^2} \nabla \nabla \cdot \boldsymbol{x}\right] G \mathrm{d}S \quad (22)$$

$$\tilde{K}(\boldsymbol{x}) = \oint_s \boldsymbol{x} \times \nabla G \mathrm{d}S \quad (23)$$

where G is the Green's function, and the integration in the equation above has remove the contribution of the singular point. The key process of MoM is solving the modal Green's function g_n which can be expressed as

$$g_n = \int_0^{\pi} \frac{e^{-jkR_0}}{R_0} \cos n\phi \, d\phi \qquad (24)$$

$$R_0 = \sqrt{\rho^2 + \rho'^2 - 2\rho\rho' \cos\phi + (z - z')^2} \qquad (25)$$

For the traditional MoM, the modal Green's function has to be evaluated by numerical method, hence it is time consuming when the radius of the BOR is large. In this section, fast inhomogeneous plane wave algorithm (FIPWA) is applied to accelerate the computation of the MoM for bodies of revolution. Based on Weyl Identity[9-10], the Green's function can be expressed as

$$\frac{e^{-jkr_{ji}}}{r_{ji}} = -j\int_0^{\infty} dk_\rho \frac{k_\rho}{k_z} J_0(k_\rho \rho_{ji}) e^{-jk_z |z_{ji}|} = \frac{-jk}{2\pi}\int_0^{2\pi} dv \int_{HSIP} du \sin u \cdot e^{-jk\boldsymbol{k}\cdot \boldsymbol{r}_{ji}} \qquad (26)$$

where $\boldsymbol{k} = k(\hat{\boldsymbol{x}} \sin u \cos v + \hat{\boldsymbol{y}} \sin u \sin v + \hat{\boldsymbol{z}} \cos u)$, $k_\rho = k\sin u$, $k_z = k\cos u$, $\boldsymbol{r}_{ji} = \boldsymbol{r}_j - \boldsymbol{r}_i$. Here $\boldsymbol{r}_i$ is the source point and $\boldsymbol{r}_j$ is the field point. In the following part, they are also named sub-scatterers. The integration of the variable u in Equation (26) is computed along the half Sommerfeld integration path (HSIP) in Figure 3. Equation (26) can be viewed as the summation of the inhomogeneous plane waves in different directions, which are expressed by $\boldsymbol{k}(u, v)$, and weighted by $\sin u$.

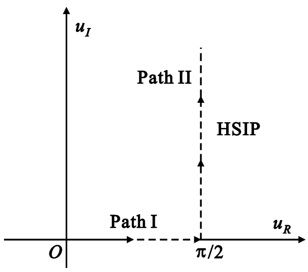

Fig.3 The Sommerfeld integration path on the complex u plane
图 3 复平面上的 Sommerfeld 积分路径

In order to realize the Fast Inhomogeneous Plane Wave Algorithm (FIPWA), the basis functions are divided into groups. Here we call $\boldsymbol{r}_m$ and $\boldsymbol{r}_{m'}$ are the centers of the groups which contain the source point $\boldsymbol{r}_j$ and field point $\boldsymbol{r}_i$ respectively. As shown in Figure 4, $\boldsymbol{r}_{ji} = \boldsymbol{r}_{jm} + \boldsymbol{r}_{mm'} + \boldsymbol{r}_{m'i}$. Equation (26) can be rewritten as

$$\frac{e^{-jkr_{ji}}}{r_{ji}} = \frac{-jk}{2\pi}\int_0^{2\pi} dv \int_{SIP} du \sin u \cdot e^{-jk\hat{k}\cdot \boldsymbol{r}_{jm}} \cdot e^{-jk\hat{k}\cdot \boldsymbol{r}_{mm'}} \cdot e^{jk\hat{k}\cdot \boldsymbol{r}_{im'}} \qquad (27)$$

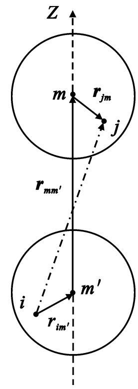

Fig.4 The field point and the source point
图 4 场点与源点位置分布

The basis functions are divided into M groups along the z direction as shown in Figure 5. In this way, the factor $\boldsymbol{r}_{mm'}$ has z component only. This character will make the integrand decay exponentially away from the real axis in the complex u plane.

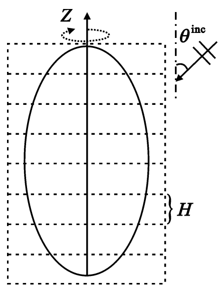

Fig.5 The BOR is divided into groups
图 5 旋转体分组示意图

Equation (26) can be rewritten as

$$\frac{e^{-jkr_{ji}}}{r_{ji}} = \int_0^{2\pi} dv \int_{HSIP} du \cdot f(u) B_{jm}(u, v) e^{-jkz_{mm'}\cos u} B_{m'i}(u, v) \qquad (28)$$

where

$$f(u) = \frac{k}{2j}\sin u \qquad (29)$$

$$B_{jm}(u, v) = e^{-jk\hat{k}\cdot \boldsymbol{r}_{jm}} \qquad (30)$$

$$B_{m'i}(u, v) = e^{-jk\hat{k}\cdot \boldsymbol{r}_{m'i}} \qquad (31)$$

Here the $B_{jm}(u, v)$ and $B_{m'i}(u, v)$ represent the radiation and receiving patterns for the field and source groups, respectively. And $f(u)$ can be considered as the weight function. Both $B_{jm}(u, v)$ and $B_{m'i}(u, v)$ are the inhomogeneous plane wave as u is complex. With proper numerical methods for u and v, the integral can be expressed as

$$\frac{\mathrm{e}^{-\mathrm{j}kr_{ji}}}{r_{ji}} = \sum_{s_2}\sum_{s_1} B_{jm}(u_{s_1}, v_{s_2}) T_{mm'}(u_{s_1}, v_{s_2}) B_{m'i}(u_{s_1}, v_{s_2}) = \sum_{\Omega_s} B_{jm}(\Omega_s) T_{mm'}(\Omega_s) B_{m'i}(\Omega_s) \quad (32)$$

where

$$\Omega_s = (u_{s_1}, v_{s_2}) \quad (33)$$

$$T_{mm'}(\Omega_s) = T_{mm'}(u_{s_1}, v_{s_2}) = \omega_1\omega_2 \frac{-\mathrm{j}k}{2\pi} \sin u_{s_1} \mathrm{e}^{-\mathrm{j}kz_{mm'}\cos u_{s_1}} \quad (34)$$

The detail of the FIPWA can be found in Reference [5-6].

2.4 FEM-FIPWA for BOR

The currents $\boldsymbol{J}$ and $\boldsymbol{M}$ are defined as

$$\boldsymbol{M}(\rho, \phi, z) = \sum_{m=-\infty}^{\infty} [\boldsymbol{E}_{t,m}(\boldsymbol{r}) + \hat{\phi} E_{\phi,m}(\boldsymbol{r})] \times \hat{n} \mathrm{e}^{\mathrm{j}m\phi} = \sum_{m=-\infty}^{\infty} \left[\sum_{i=1}^{N_s^b} e_{m,i}^t P_i - \sum_{i=1}^{N_n^b} e_{m,i}^{\phi} \frac{T_i}{\rho} \hat{t} \right] \mathrm{e}^{\mathrm{j}m\phi}, \boldsymbol{r} \in S \quad (35)$$

$$\boldsymbol{J}(\rho, \phi, z) = \sum_{m=-\infty}^{\infty} \hat{n} \times [\boldsymbol{H}_{t,m}(\boldsymbol{r}) + \hat{\phi} H_{\phi,m}(\boldsymbol{r})] \mathrm{e}^{\mathrm{j}m\phi} = \sum_{m=-\infty}^{\infty} \left[-\sum_{i=1}^{N_s^b} h_{m,i}^t \hat{\phi} P_i + \sum_{i=1}^{N_n^b} h_{m,i}^{\phi} \frac{T_i}{\rho} \hat{t} \right] \mathrm{e}^{\mathrm{j}m\phi}, \boldsymbol{r} \in S \quad (36)$$

where P_i is the pulse basis function and T_i is the traditional triangle basis function. Combining the FEM part (interior region) and FIPWA (boundary), the matrix equation can be derived as

$$\begin{bmatrix} A_{tt}^{ii} & A_{t\phi}^{ii} & A_{tt}^{ib} & A_{t\phi}^{ib} & 0 & 0 \\ A_{\phi t}^{ii} & A_{\phi\phi}^{ii} & A_{\phi t}^{ib} & A_{\phi\phi}^{ib} & 0 & 0 \\ A_{tt}^{bi} & A_{t\phi}^{bi} & A_{tt}^{bb} & A_{t\phi}^{bb} & G_{tt}^{bb} & G_{t\phi}^{bb} \\ A_{\phi t}^{bi} & A_{\phi\phi}^{bi} & A_{\phi t}^{bb} & A_{\phi\phi}^{bb} & G_{\phi t}^{bb} & G_{\phi\phi}^{bb} \\ 0 & 0 & Z_{\phi\phi}^{b} & Z_{\phi t}^{b} & Z_{\phi\phi}^{a} & Z_{\phi t}^{a} \\ 0 & 0 & Z_{t\phi}^{b} & Z_{tt}^{b} & Z_{t\phi}^{a} & Z_{tt}^{a} \end{bmatrix} \cdot \begin{bmatrix} e_t^i \\ e_\phi^i \\ e_t^b \\ e_\phi^b \\ h_t^b \\ h_\phi^b \end{bmatrix} = \begin{bmatrix} 0 \\ 0 \\ 0 \\ 0 \\ V_\phi \\ V_t \end{bmatrix} \quad (37)$$

The details of the matrix elements can be found in Reference [4-6]. The boundary currents and fields can be derived by solving the equation above, and the far field also can be solved. In the next section, two numerical results will be given to demonstrate the validity and the efficiency of the proposed method.

3 Numerical Results

In this section, two numerical results are presented to show the validity of the proposed FEM-FIPWA method. All problems are solved on the same computer (Intel Core2 DuoCPU P8400@2.26GHz with 1.92GB RAM) in order to make a fair comparison, with only one core being used.

3.1 An inhomogeneous dielectric sphere with two layer medium

As shown in Figure 6, an inhomogeneous dielectric sphere is computed. The sphere is excited by the plane wave with horizontal polarization ($\theta^{\mathrm{inc}} = 0^0, \phi^{\mathrm{inc}} = 0^0, \lambda = 2$ m). The total number of the unknowns is about 40 000. The bistatic RCS is shown in Figure 7, the result of FEM-BI (or FEM-FIPWA) agrees well with analytical result.

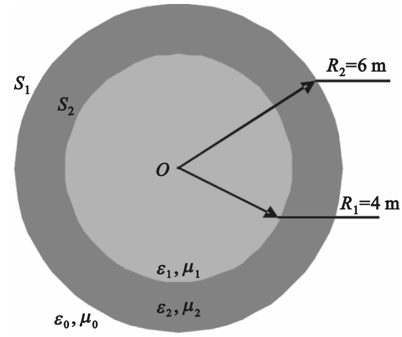

Fig.6 An inhomogeneous dielectric sphere with two-layer medium

图 6 非均匀双层介质球结构

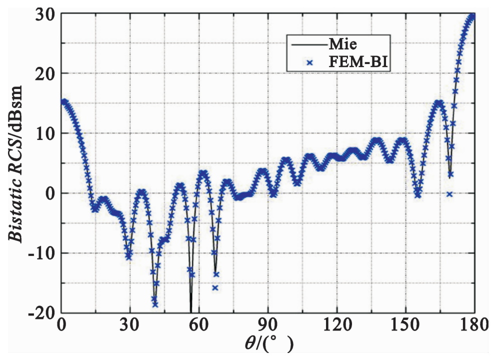

Fig.7 The bistatic RCS of the dielectric sphere result by FEM-BI compared with analytic result

图 7 介质球双站 RCS 的计算结果比较图

3.2 An inhomogeneous dielectriccylinder

The numerical result proposed above shows the accuracy of FEM-FIPWA for BOR problems. In this section, a more complex example is shown to verify the efficiency of proposed method mentioned in this paper. As shown in-Figure 8, there are seven layered medium. The thickness of the six inner medium is 0.2 m and the height is 2.6 m. The thickness of the outer medium is 0.3 m, and the height is 2 m. The cylinder is excited by the plane wave with horizontal polarization ($\theta^{\mathrm{inc}} = 90°, \phi^{\mathrm{inc}} = 0°, \lambda = 0.5$ m). The number of the total unknowns is more than 100 000 in this 2-D mesh. The field distribution derived by FEM-BI is compared with Wavenology which is a famous commercial EM software in USA. As shown in Figure 9, the results agree well with each other.

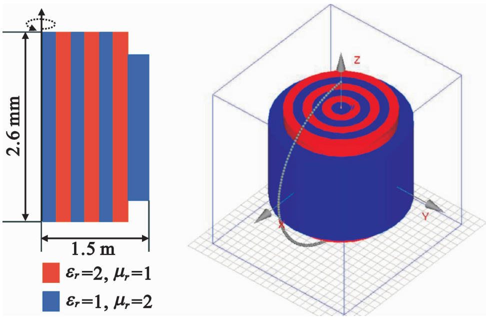

Fig.8 The geometry of the inhomogeneous dielectric cylinder
图 8 非均匀介质柱结构图

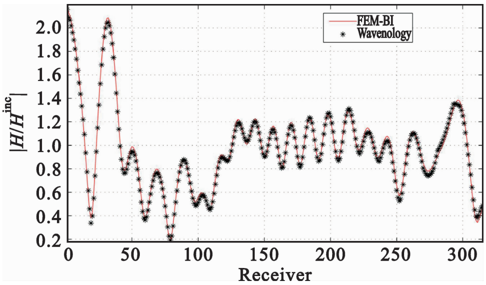

Fig.9 The field distribution of the dielectric cylinder with two different methods
图 9 两种方法计算介质柱的场分布结果比较

As shown in Table 1, the memory requirements and CPU times for FEM-MoM and FEM-FIPWA are compared.

Table 1 The comparison between FEM-MoM and FEM-FIPWA
表 1 FEM-MoM 与 FEM-FIPWA 计算比较

Method	Memory requirement/MB	CPU time/s
FEM-FIPWA	165.6	2 258
FEM-MoM	171.9	5 750

4 Conclusion

In this paper, hybrid FEM and FIPWA technique is applied to solve the BOR scattering problem. In this FEM-FIPWA method, the problem is separated into interior and exterior problems. In the interior region, FEM based on hybrid edge-based and node-based elements is used to present the electric field. In the exterior region, boundary integration (BI) is used as the exact boundary condition. Triangular and pulse basis functions are used for representing the electric and magnetic fields on the boundary. FIPWA is added for the BI part. The proposed method can solve large scale bodies of revolution with inhomogeneous, composite materials efficiently.

References:

[1] Andreasen M G. Scattering from bodies of revolution [J]. IEEE Transactions on Antennas and Propagation, 1965, 13 (2): 303 – 310.

[2] Mautz J R, Harrington R F. Electromagnetic coupling to a conducting body of revolution with a homogeneous material region [J]. Electromagnetics, 1982(2): 257 – 308.

[3] Medgyesi-Mitschg L N, Putnam J M. Electromagnetic scattering from axially inhomogeneous bodies of revolution[J]. IEEE Transactions on Antennas and Propagation, 1984, 32(8): 797 – 806.

[4] Rui Xi. Finite element method for inhomogeneous axisymmetric resonators[J]. Telecommunication Engineering, 2012, 52 (1): 105 – 110.

[5] Rui X, Hu J, Liu Q H. Fast Inhomogeneous Plane Wave Algorithm for Scattering from PEC Body of Revolution[J]. Microwave and Optical Technology Letters, 2010, 52(8): 1915 – 1922.

[6] Rui X, Hu J, Liu Q H. Higher order finite element method for inhomogeneous axisymmetric resonators [J]. Progress In Electromagnetics Research B, 2010, 21: 189 – 201.

[7] Morgan M A, Mei K K. Finite-element computaion of scattering by inhomogeneous penetrable bodies of revolution [J]. IEEE Transactions on Antennas and Propagation, 1979, 27 (2): 202 – 214.

[8] Lee J F, Wilkins G, Mittra R. Finite-element analysis of axisymmetric cavity resonator using a hybrid edge element technique [J]. IEEE Transactions on Microwave Theory Technique, 1993, 41(11): 1981 – 1987.

[9] Chew W C. Waves and Fields in Inhomogeneous Media [M]. New York: Van Nostrand Reinhold Co. Ltd., 1990.

[10] Hu B, Chew W C, Michielssen E, et al. Fast inhomogeneous plane wave algorithm for the fast analysis of two-dimensional scattering problem [J]. Radio Sciences, 1999, 34(4): 759 – 772.

Biography:

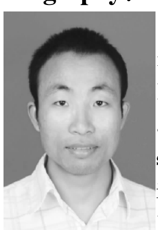

RUI Xi was born in Liyang, Jiangsu Province, in 1983. He received the B.S. degree and the Ph.D. degree from University of Electronic Science and Technology of China in 2005 and 2010, respectively. From 2008 to 2010, he has been working with Prof. Q. H. Liu as a visiting scholar in Duke University. He is now an engineer. His research interests include computational electromagnetic and RF stealth.

Email: uestcruixi@gmail.com

芮 锡(1983—),男,江苏溧阳人,分别于 2005 年和 2010 年获电子科技大学学士学位和博士学位,2008 ~ 2010 年在美国北卡州杜克大学做访问,现为工程师,主要研究方向为电磁计算与射频隐身。